Journal of Advanced Mechanical Design, Systems, and Manufacturing

Vol. 2, No. 3, 2008

Development of a Compact Maglev Centrifugal Blood Pump Enclosed in a Titanium Housing*

Chi Nan PAI**, Tadahiko SHINSHI***, Junichi ASAMA†, Setsuo TAKATANI†† and Akira SHIMOKOHBE***

** Interdisciplinary Graduate School of Science and Engineering, Tokyo Institute of Technology

*** Precision and Intelligence Laboratory, Tokyo Institute of Technology

4259 Nagatsuta Midori-ku, Yokohama 226-8503, Japan

E-mail: shinshi@pi.titech.ac.jp

†Department of Electrical Engineering, Tokyo University of Science

††Institute of Biomaterials and Bioengineering, Tokyo Medical and Dental University

Abstract

A compact centrifugal blood pump consisting of a controlled two-degrees-of-freedom radial magnetic bearing and a brushless DC motor enclosed in a titanium housing has been developed for use as an implantable ventricular assist device. The magnetic bearing also supports axial and angular motions of the impeller via a magnetic coupling. The top housing is made of pure titanium, while the impeller and the stator are coated with pure titanium and Ti-6Al-7Nb, respectively, to improve the biocompatibility of the pump. The combination of pure titanium and titanium alloy was chosen because of the sensitivity of eddy current type displacement sensors through the intervening conducting wall. The dimensions of the pump are 69.0 mm in diameter and 28.5 mm in height. During a pump performance test, axial shifting of the impeller due to hydraulic forces led to variations in the rotational positioning signal, causing loss of control of the rotational speed. This problem was solved by conditioning the rotational positioning signal. With a flow rate of 5 l/min against a head pressure of 100 mmHg, the power consumption and efficiency of the pump were 5.5 W and 20%, respectively. Furthermore, the hemolysis of the blood pump was 43.6% lower when compared to that of a commercially available pump.

Key words: Centrifugal Blood Pump, Magnetic Bearing, Biocompatibility, Eddy Current Type Displacement Sensor, Hydraulic Force

1. Introduction

In the past decade, significant progress in the research and development of blood pumps has been achieved and the use of blood pumps has gained acceptance as an elective therapy for heart failure, in place of heart transplants. The lifetime needed for blood pump circulatory support has increased and consequently, the requirements of these pumps, in terms of their durability and reliability, blood damage, biocompatibility, incidence of complications through infection and overall quality of life, have become stricter, and this has lead to the development of fully implantable blood pumps [(1)].

In our laboratory, a prototype maglev centrifugal blood pump called MedTech Heart, consisting of a controlled two-degrees-of-freedom radial magnetic bearing (MB), a built-in brushless DC motor and a plastic housing was developed [(2)]. Since the impeller in this pump is magnetically levitated, there is no contact between the rotating and stationary parts, increasing its durability and decreasing the blood damage level [(3)].

In order to be fully implantable, those surfaces in contact with biological tissue should

*Received 20 Dec., 2007 (No. 07-0841)
[DOI: 10.1299/jamdsm.2.343]

be made of biocompatible material. Titanium and some alloys of titanium are well known biomaterials which are present not only in heart valves and vascular stents [4], [5], but also in maglev centrifugal blood pumps, such as HeartMate III (Thoratec Corp, U.S.A.) [6], [7], and DuraHeart (TerumoHeart Inc., U.S.A.) [7], [8]. Although both these blood pumps have a titanium housing, there is no published reference on the influence of this housing on the sensitivity of the position sensors for the MB, on the stability of the MBs, nor on the energy losses of the drive motor.

MedTech Heart uses eddy current type displacement sensors to sense the radial position of the impeller and to provide the MB with this radial positioning signal, as shown in Fig. 1. When titanium, a conducting material, is used for the pump housing, there is a titanium frame (stator wall) between the displacement sensor and its target (impeller cover). The generation of eddy currents in the titanium frame of the stator wall distort the magnetic flux between the displacement sensor and the sensor target, affecting its sensitivity, as shown in Fig. 2.

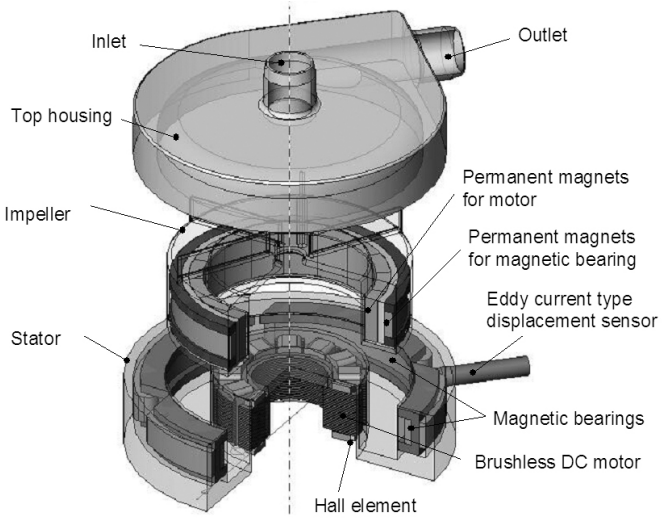

Fig. 1 Exploded view of MedTech Heart

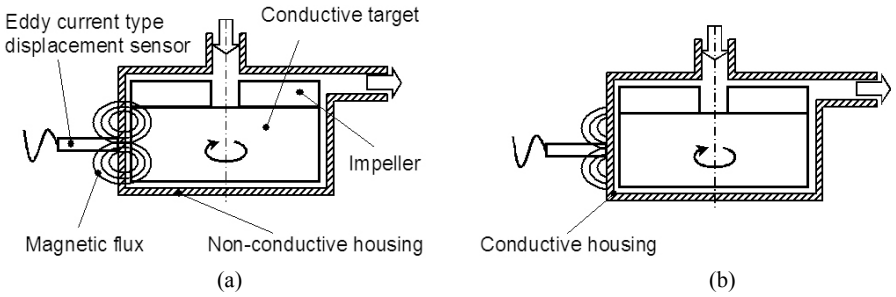

Fig. 2 Sensitivity of the displacement sensor (a) with a non-conducting housing and (b) through an intervening conducting housing

In addition, there is a titanium frame between the moving and stationary parts of the MB and the brushless DC motor. Eddy currents induced by MBs on the stator wall may cause variations in the dynamic characteristics of the MBs, affecting their stability. Besides, the existence of eddy current losses may also increase the power consumption of the motor, decreasing its efficiency.

Moreover, the axial and angular motions of the impeller of the MedTech Heart are passively supported by a magnetic coupling. This configuration reduces the number of displacement sensors and electromagnets needed for the MB, but leads to lower axial stiffness compared to the radial direction, which is actively controlled [2]. The lower axial stiffness, associated with hydraulic forces inside the pump, causes axial shifting of the

impeller. Three Hall elements installed at the bottom of the stator measure the magnetic flux of the permanent magnets (PMs) located inside the impeller. This signal, including information on the rotational angle of the impeller, is feedbacked to control the rotation of the impeller. Axial shifting of the impeller causes variation of the distance between the PMs and the Hall elements, leading to variations in the amplitude of the feedback signal, and a consequent loss of control of the rotational speed.

In this article, we describe the realization of a maglev centrifugal blood pump enclosed in a titanium housing, which has the potential to be a fully implantable blood pump. In order to substitute the plastic housing of the MedTech Heart with a titanium one, the influence of the eddy currents on the displacement sensors, and the control of the MBs and the motor were evaluated. Furthermore, to avoid loss of control of the rotational speed due to axial shifting of the impeller, a method for compensating for weakened signals from the Hall elements was investigated. Finally, the pump performance was evaluated and its hemolytic characteristics were compared with the commercially available Bio-Pump BPX-80 (Medtronic Biomedicus Inc., U.S.A.), which is widely used in circulatory support and as hemolysis test control [9].

2. Sensitivity and Dynamics of an Eddy Current Type Displacement Sensor Through a Conducting Wall

2.1 Method for evaluating the sensitivity and dynamics of the displacement sensor

In order to evaluate the influence of a conducting frame between the eddy current type displacement sensor (PU-03A, Applied Electronics Corp., Japan) and its target, three types of titanium frames with different composition and thickness (t), pure titanium with t = 0.3 mm, Ti-6Al-7Nb with t = 0.3 mm and t = 0.5 mm, were used to replicate the stator wall (inner cover of the bottom housing) and the target cover (impeller cover). In addition, sets of measurements using three different types of titanium frame as the target cover, but without a stator wall, were performed. As a result, twelve different combinations of stator wall and target cover were evaluated, as shown in Table 1.

Ti-6Al-7Nb was chosen as a housing material due to its good biocompatibility properties, different resistivity compared with pure titanium, and the lower cytotoxicity characteristics of niobium compared with vanadium, which is present in Ti-6Al-4V and widely used as biomedical alloy [4], [10]. The resistivities of pure titanium and of Ti-6Al-7Nb, measured using a resistivity meter (Loresta GP - MCP T600, Dia Instruments, Japan), were 4.55×10^{-7} Ω.m and 1.69×10^{-6} Ω.m, respectively.

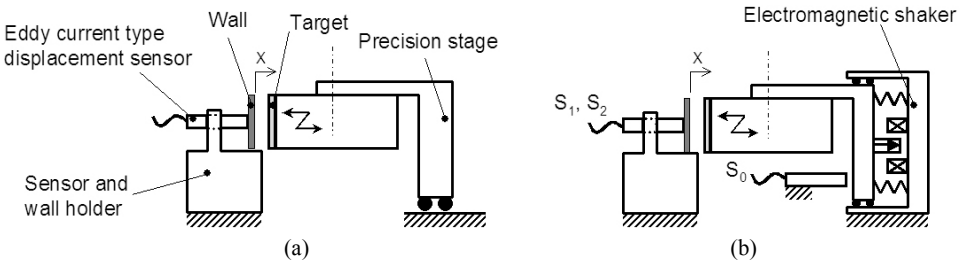

Fig. 3 Experimental setup to evaluate (a) the sensitivity and (b) the dynamic characteristics of an eddy current type displacement sensor through a conducting wall

In the experimental setup, the displacement sensor was fixed to a holder, as shown in Fig. 3a, with the sensor head attached to the conducting stator wall, and the target cover fixed to a precision stage with the capability of providing micrometrical displacement to change the gap between the displacement sensor and the target.

Defining the origin of the displacement (x) of the target as when the target cover touches the conducting stator wall, the sensor output signal was obtained with respect to

variations in x, and the sensitivity of the signal was measured for different combinations of the stator wall and target cover.

To evaluate the frequency characteristics of the displacement sensor, a similar experimental setup was used, oscillating the target cover with an electromagnetic shaker as shown in Fig. 3b. In this case, the frequency response of the displacement sensor was obtained using a frequency response analyzer (FRA5095, NF Corp., Japan). In Fig. 3b, S_1 is the target displacement signal through the stator wall, S_2 is the direct target displacement signal without a stator wall, and S_0 is the displacement signal of the base of shaker. The influence of the titanium stator wall, represented by S_1/S_2, was calculated using the measured data of S_1/S_0 and S_2/S_0.

2.2 Experimental results

Figure 4a shows the displacement sensor output with respect to the displacement of the target, using pure titanium (t = 0.3 mm) as the target material. Table 1 shows the sensitivities of the displacement sensor for all twelve combinations of stator wall and target cover. Since the sensor output was nonlinear and the designed fluid gap between the impeller and MB stator was 0.25 mm, a linear regression was performed for the data in the range of x = 0.15 ~ 0.35 mm and the value of the sensitivity was obtained from the approximated equation, as shown in Fig. 4a.

Table 1 Sensitivity of the eddy current type displacement sensor [Unit:V/mm]

Target \ Wall	Ti (t = 0.3 mm)	Ti-6Al-7Nb (t = 0.5 mm)	Ti-6Al-7Nb (t = 0.3 mm)	Without wall
Ti (t = 0.3 mm)	#1 -0.06	#2 -0.72	#3 -3.04	#4 8.23
Ti-6Al-7Nb (t = 0.5 mm)	#5 -0.07	#6 -0.55	#7 -1.99	#8 9.90
Ti-6Al-7Nb (t = 0.3 mm)	#9 -0.01	#10 -0.53	#11 -2.23	#12 8.53

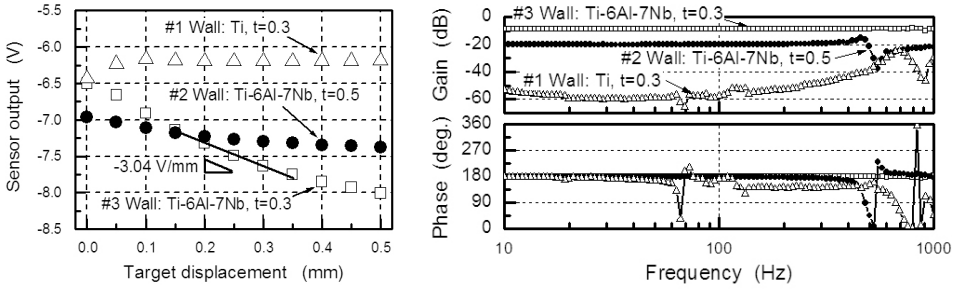

(a) (b)

Fig. 4 (a) Signal output and (b) frequency response S1/S2 of the displacement sensor with a 0.3 mm thick Ti target

Of all the combinations, except those without a conducting wall, the one using Ti-6Al-7Nb as the wall material and pure titanium as the target material, both 0.3 mm thick, (#3), presented the highest sensitivity. Besides, the sign of the sensitivity became inverted when a titanium frame was used for the stator wall.

The frequency response $S_1(s)/S_2(s)$ of the displacement sensor using 0.3 mm thick pure titanium as the target material, with different compositions and thicknesses of the stator wall, is presented in Fig. 4b. For combination #3, there was neither loss of gain nor phase delay for frequencies below 1 KHz, whereas combinations #1 and #2, had both gain

changes and phase delays at 10 Hz and 400 Hz, respectively. Since the control bandwidth of the MB is several hundred hertz, combination #3 presents sufficient dynamic characteristics for control of the MBs.

2.3 Discussion

The main reason for the high sensitivity of the eddy current type displacement sensor through the 0.3 mm thick Ti-6Al-7Nb wall is that the magnetic flux through it to the target is sufficiently high. The penetration depth of a magnetic flux in a conducting material, known as skin depth (d), is given by equation (1):

$$d = \sqrt{\frac{\rho}{\pi f \mu}} \tag{1}$$

where ρ is the resistivity of the conductor (Ω.m), f is the frequency of the magnetic flux (Hz) and μ is the absolute magnetic permeability of the conductor (H/m). When the conducting material is thicker than the skin depth, the field is blocked and there is no passage of the magnetic flux through it.

Using the measured resistivities of pure titanium and Ti-6Al-7Nb, and with the carrier frequency of the displacement sensor f = 2MHz, the skin depth of each material is 0.24 and 0.46 mm, respectively. For the 0.3 mm thick Ti-6Al-7Nb stator wall, the wall thickness is less than the skin depth, so the magnetic flux easily passes through the stator wall and a high sensitivity of the displacement sensor can be obtained. On the other hand, for 0.3 mm thick pure titanium and 0.5 mm thick Ti-6Al-7Nb, the thickness is larger than the respective skin depths, and as consequence, the magnetic flux decays significantly, drastically reducing the sensitivity of the sensor.

Of the various target covers used with the 0.3 mm thick Ti-6Al-7Nb stator wall, the 0.3 mm thick pure titanium gave the highest gain because its resistivity is lower compared to that of Ti-6Al-7Nb. Therefore, the eddy current generated on the surface of the target was the largest, providing the highest sensitivity for the displacement sensor.

To investigate inversion of the sign of the sensitivity when a titanium wall was set between the eddy current type displacement sensor and the titanium target, an LCR meter (3532-50 HiTester, Hioki, Japan) was used to measure the resistance (R), inductance (L) and capacitance (C) of the displacement sensor, in the same experimental setup shown in Fig. 3a. In this process, the LCR meter measurement frequency was 2 MHz, the same as the carrier frequency of the displacement sensor. Figures 5a, 5b and 5c show the variations in resistance, inductance and capacitance with respect to the target displacement for combination #3.

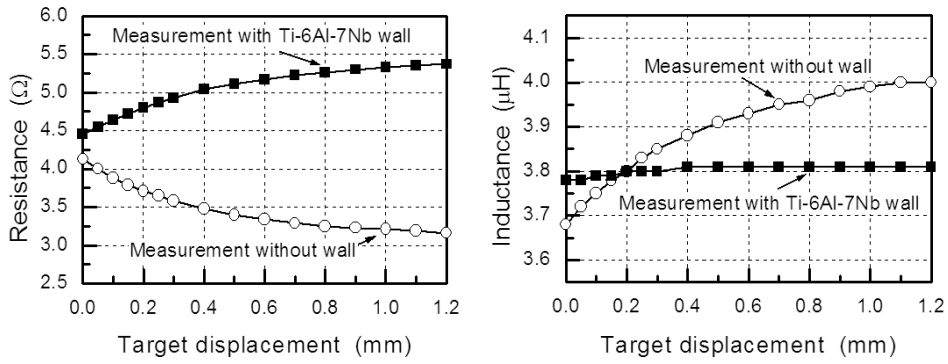

(a) (b)

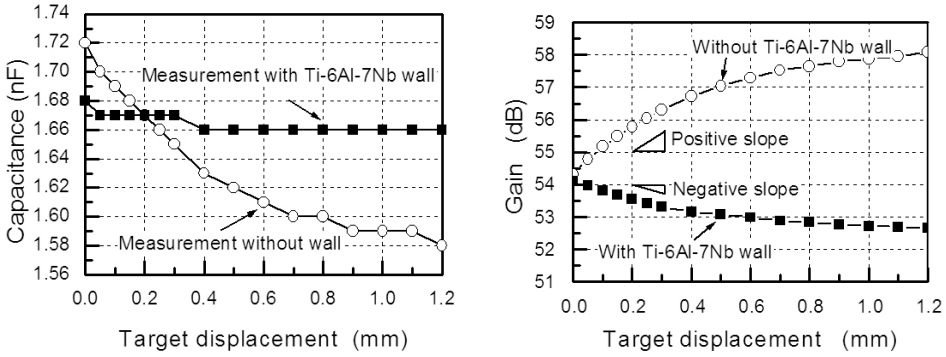

(c) (d)

Fig. 5 Measured values of (a) resistance, (b) inductance and (c) capacitance of the displacement sensor, and (d) calculated gains of the transfer function $Z(s)$ using these data

Considering the equivalent circuit of the displacement sensor, the transfer function $Z(s)$ of the impedance $Z = V / I$ of this equivalent circuit is given by equation (2)

$$Z(s) = \frac{V(s)}{I(s)} = \frac{Ls + R}{LCs^2 + RCs + 1} \tag{2}$$

where V and I are the voltage and current of the sensor coil, respectively.

Using the measured resistance, inductance and capacitance and calculating the gain of the transfer function $Z(s)$ at a frequency of 2 MHz, Fig. 5d shows the inversion of the slope of the impedance with respect to the displacement (x) of the target.

3. Fabrication and Evaluation of a Maglev Centrifugal Blood Pump with a Titanium Housing

3.1 Configuration of a MedTech Heart with a titanium housing

Photographs of a MedTech Heart with a titanium housing and an exploded view are shown in Fig. 6 and Fig. 1, respectively. A 0.25 mm thick Ti-6Al-7Nb wall and a 0.5 mm thick Ti cover were used for the stator and impeller, respectively. The top housing was made of pure titanium.

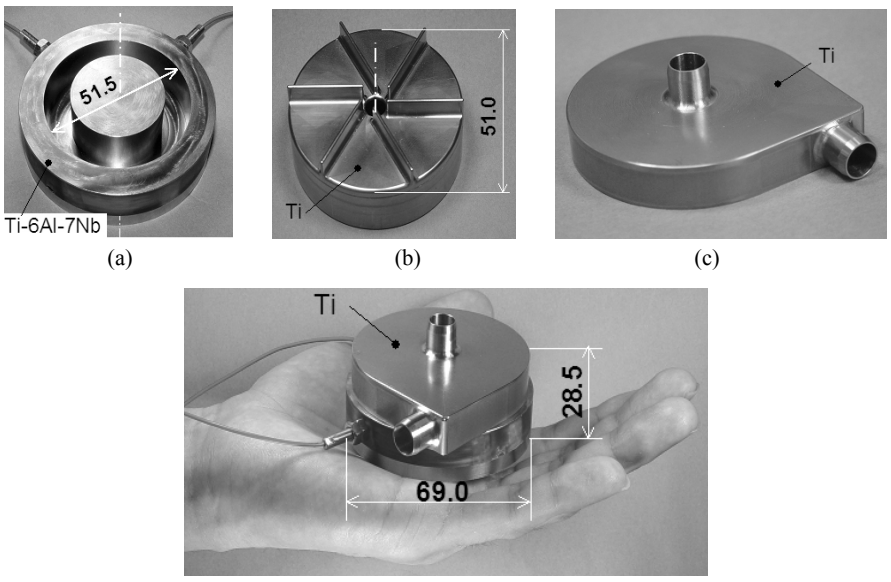

(a) (b) (c)

(d)

Fig. 6 Photographs of (a) the stator, (b) the impeller, (c) the top housing and (d) a MedTech Heart with a titanium housing

The dimensions of this centrifugal blood pump are 69.0 mm in diameter and 28.5 mm in height with a weight of 370 g and a measured priming volume of 20 ml, making it smaller and lighter than the HeartMate III, which is 69 mm in diameter, 30 mm in height and 500 g in weight [6], and the DuraHeart, which is 72 mm in diameter, 45 mm in height and 540 g in weight [7], [8]. Inside the pump, the magnetically levitated impeller is 51 mm in diameter and 98 g in weight.

The two-degrees-of-freedom controlled MB system is comprised of four electromagnets located in the stator and a sandwich of two iron rings and a PM ring embedded inside the impeller. The impeller radial displacement signal is feedbacked by two eddy current type displacement sensors located between the electromagnets, allowing the MB to actively control the radial motion of the impeller and to passively support both the axial and angular motions [2]. The titanium cover of the impeller is used as the displacement sensor target.

An internal brushless DC motor located in the central part of the pump generates the rotation of the impeller. Sixteen PMs embedded in the impeller are arranged in a Halbach array configuration [11], generating eight magnetic poles in the inward direction [12]. The motor stator has twelve teeth and three phase windings. Three Hall elements are set under three consecutive teeth to detect the magnetic poles of the Halbach PM array and to feedback the rotational position of the impeller to control the motor using a PWM driver (UMXG-8, Waco Giken Co. Ltd, Japan).

The PWM driver requires bi-phasic rotational positioning signals (V_a and V_b) with an amplitude of 1.8 ± 0.2 V and an offset of 2.5 V, and a rotational reference signal (ω_r) in order to control the rotational speed (ω) of the impeller. The Hall element signals (V_u, V_v and V_w) are converted to V_a and V_b by a signal converter, as shown in Fig. 7. The signal conversion is represented by the following equation (3):

$$\begin{pmatrix} V_a \\ V_b \end{pmatrix} = \begin{pmatrix} K_a & -K_a/2 & -K_a/2 \\ 0 & \sqrt{3}K_b/2 & -\sqrt{3}K_b/2 \end{pmatrix} \begin{pmatrix} V_u \\ V_v \\ V_w \end{pmatrix} + \begin{pmatrix} 2.5 \\ 2.5 \end{pmatrix} \tag{3}$$

where K_a and K_b are correction factors, assumed to be constant, used to adjust the rotational positioning signal required by the PWM driver.

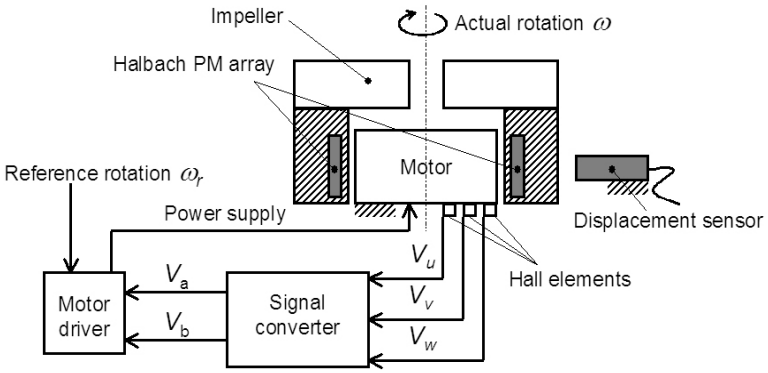

Fig. 7 Rotational control system

3.2 Evaluation of the stability of the magnetic bearing

3.2.1 Method

To evaluate the influence of eddy currents on the stability of the MB, the displacement sensor noise, the positioning resolution and the dynamic characteristics of the MB were investigated. The sensor noise was evaluated using the same experimental setup shown in Fig. 3a, with a 0.25 mm thick Ti-6Al-7Nb stator wall, the same as used in the pump housing, a 0.5 mm thick target frame positioned at x = 250 μm, the designed pump fluid

gap, and a sampling frequency of 10 KHz. The signal was compared with the one measured directly without the stator wall. The positioning resolution of the MB was obtained by applying a step reference to the MB control system[13] and measuring stepwise displacements of the impeller in the x direction, with the impeller levitated in air, without rotation.

The dynamic characteristics were evaluated through a frequency response analyzer. The influence of the titanium wall was observed by measuring the transfer function from the current $I(s)$ to the displacement signal $X(s)$ in air and by comparing the frequency response of the MB with a titanium wall to one with a plastic wall. The transfer function is shown in equation (4)

$$\frac{X(s)}{I(s)} = \frac{K_i}{Ms^2 + Cs - K_x} \tag{4}$$

where K_i is the current-force factor, M is the mass of impeller, C is the damping factor and K_x is the radial stiffness of the MB.

3.2.2 Results and discussion

The sensor noise was 0.61 μm (3σ) and 0.24 μm (3σ) with and without the Ti-6Al-7Nb wall, respectively, as shown in Fig. 8. Eddy currents on the surface of the stator wall decrease the sensitivity of the displacement sensor, and increase the ratio of the sensor noise to signal output, leading to higher sensor noise in terms of displacement, when a titanium wall is set between the sensor and the target.

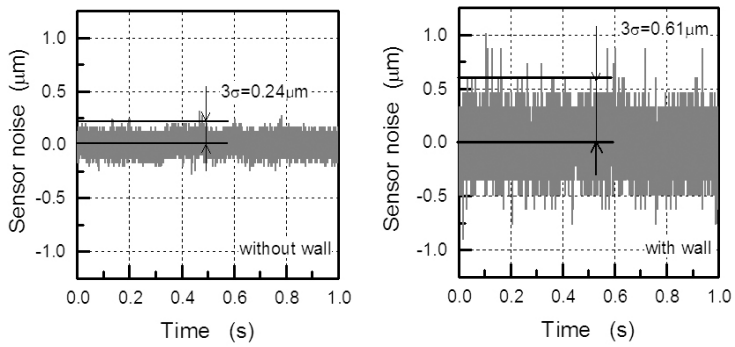

Fig. 8 Displacement sensor noise (a) without and (b) with a Ti-6Al-7Nb wall

The step positioning result showed that the positioning resolution of the MB was 0.75 μm and the displacement vibration was 0.7 μm (3σ), as shown in Fig. 9a. This positioning resolution is sufficient for a MB to be used in a blood pump with fluid gap of 250 μm.

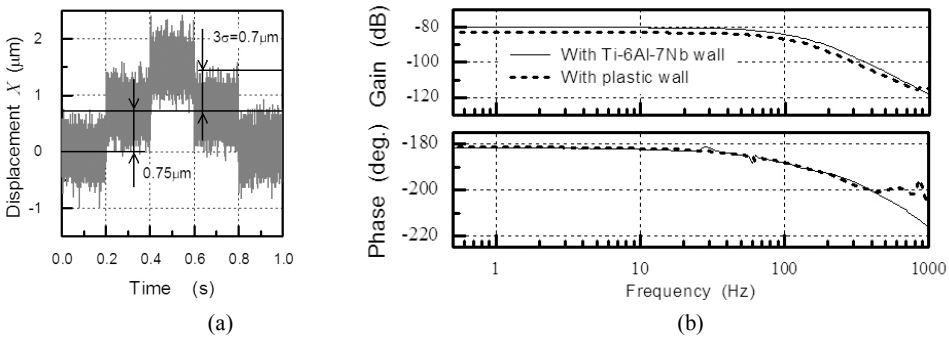

Fig. 9 (a) Positioning resolution and (b) frequency response X(s)/I(s) of a magnetic bearing through an intervening Ti-6Al-7Nb wall

The dynamic characteristics of the MB in a titanium housing showed the same gain and phase shapes compared to one with a plastic housing, as shown in Fig. 9b, suggesting that

the titanium alloy wall has little influence on the dynamics of the MB. Moreover, the difference in gain curves at low frequency, suggests differences in the radial stiffness (K_x) and current-force factor (K_i) of the MBs due to assembling errors.

3.3 Evaluation of pump efficiency

The pressure-flow performance (HQ curve) and the power consumption of the pump were obtained with the pump set in a mock circulatory loop, as shown in Fig. 10, consisting of two fluid pressure sensors (KL76, Nagano Keiki Co., Japan), one connected to the inlet and the other to the outlet of the pump to measure the head pressure (H), an electromagnetic flow probe (FD-M10AY, Keyence, Japan) to measure the flow rate (Q), a screw clamp to provide variable flow resistance and a reservoir, with water used as the working fluid.

The power consumption of the prototype was due to consumption by the motor (P_{motor}) and the MB (P_{mb}), and didn't include that of the amplifiers, power supplies, sensor transducers and control electronics. P_{motor} was measured by power meters (WT210, Yokogawa Electric Corp., Japan) and P_{mb} was calculated from the voltage and current applied to the MB. The voltage was measured directly by the digital signal processor (DS1103, dSPACE GmbH, Germany) used for active control of the MB, and the current was measured using Hall-effect current sensors (LA25-NP/7, LEM, Japan).

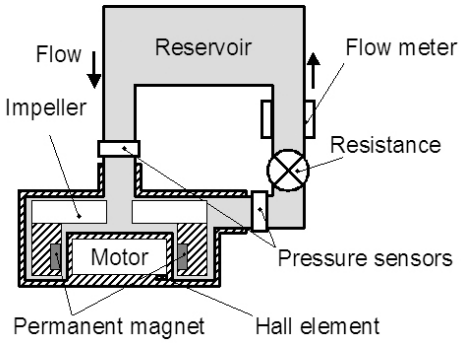

Fig. 10 Mock circulatory loop

The pump efficiency, was then calculated using data from the pump HQ curve and the power consumption, according to equation (5):

$$Efficiency = \frac{HQ}{P_{mb} + P_{motor}} \tag{5}$$

During evaluation of the pump efficiency, the rotational speed of the impeller was unable to follow the reference rotational speed when this was higher than 1500 rpm. This led to low pump efficiency, about 6.7%, when providing a flow rate of 5 l/min against a head pressure of 100 mmHg.

4. Loss of control of the rotational speed

4.1 Cause of the loss of control

As explained in the introduction, the hydraulic forces inside the pump cause variations in the amplitude of the Hall element signals and this, when the amplitude correction factors (K_a and K_b) are assumed to be constant, is reflected in the amplitude of the rotational positioning signals (V_a and V_b). In this case the signal amplitude required by the motor driver (1.8 ± 0.2 V) can no longer be satisfied, leading to a divergence of the actual (ω) from the reference rotational speed (ω_r). The actual rotational speed (ω) was estimated through FFT analysis of the radial displacement signals of the impeller, induced by the imbalance of the impeller.

4.2 Compensation method and results

In order to compensate for the variation in the rotational positioning signals (V_a and V_b), the Hall element signals were evaluated with respect to head pressure and rotational speed, using a mock circulatory loop. The relationship between the Hall element signal, head pressure and rotational speed is shown in Fig. 11. Although there was a weakening of the Hall element signal when the speed was increased, the head pressure had little influence on the variation of the signal. Using this result, the correction factors K_a and K_b depending only on the rotational speed were determined.

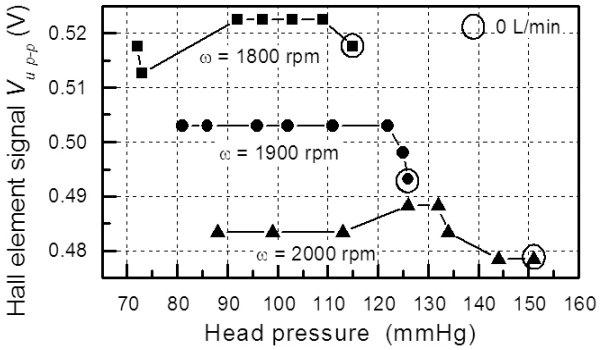

Fig. 11 Relationship between the Hall element signal, rotational speed and head pressure

The process flow to determine the appropriate values of K_a and K_b for each rotational speed is shown in Fig. 12. The process starts with $\omega_r = 0$ and the initial values of K_a and K_b for air. The Hall element signals (V_u, V_v and V_w) are converted to rotational positioning signals (V_a and V_b). If the amplitudes of these are outside the required range, 1.8 ± 0.1 V, the process is repeated with modified values of K_a and K_b. Once the requirements are satisfied, the values of K_a and K_b are saved. The rotational speed is then increased by 100 rpm and the process repeated using the modified values of K_a and K_b. This entire process is continued until the rotational speed is 2200 rpm.

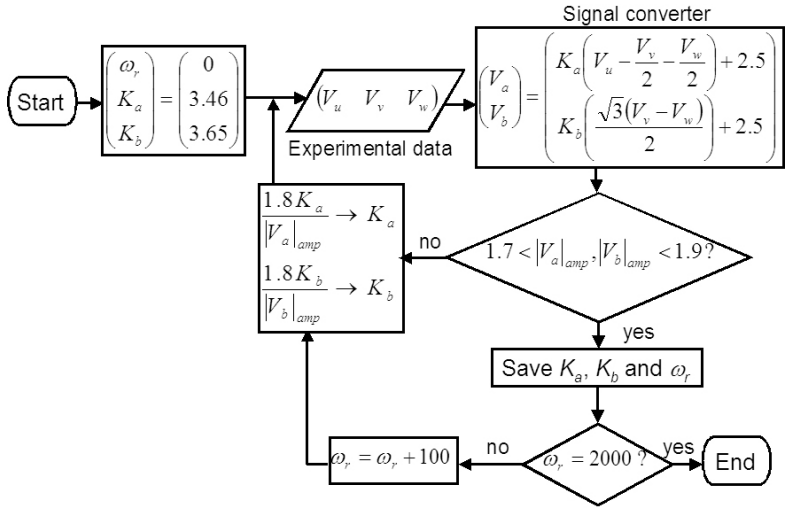

Fig. 12 Flow diagram to obtain the corresponding K_a and K_b for each rotational speed

K_a and K_b as functions of the rotational speed are shown in Fig. 13a, from which the following equations (6) were obtained to be used in the signal converter. As result, the difference between the actual and the reference rotational speeds was decreased, as shown in Fig. 13b.

$$K_a = 6.0\times10^{-7}\omega_r^{\ 2} - 5.0\times10^{-4}\omega_r + 3.7$$
$$K_b = 6.0\times10^{-7}\omega_r^{\ 2} - 5.0\times10^{-4}\omega_r + 3.5 \qquad (6)$$

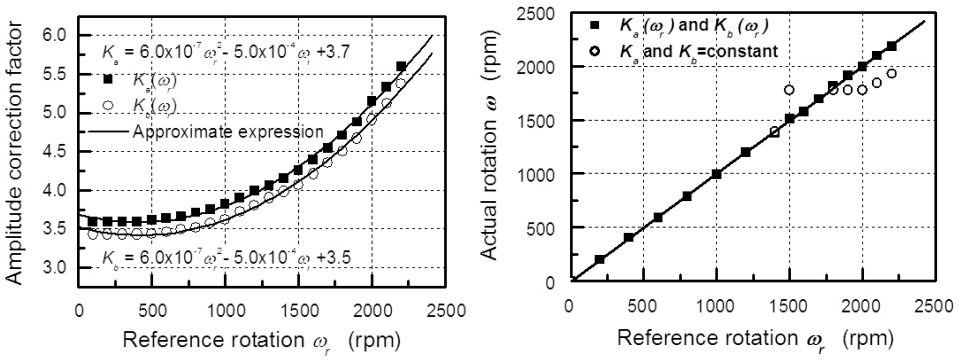

(a) (b)

Fig. 13 (a)Variation of K_a and K_b with respect to the reference rotational speed, and (b) their influence on the actual rotational speed

4.3 Discussion

The difference between the actual and reference rotational speeds is due to the position of the Hall elements at the bottom of the motor stator and the axial shifting of the impeller. Changing the location of the Hall elements doesn't solve this problem because, at the centre of the motor, the magnetic flux of motor has an influence, and at the top of the motor stator, there is the same signal range problem. The alternative is to increase the number of Hall element sensors, setting one at the top of the motor stator and another at the bottom to obtain a differential signal between them. Other alternatives not involving Hall elements include changing the magnetic bearing design to increase the axial stiffness of the impeller, and changing the pump design to decrease the hydraulic forces inside the pump.

5. Pump Performance

5.1 Pump efficiency

Using the signal conditioning algorithm and the mock circulatory loop, a MedTech Heart in a titanium housing was able to provide a flow rate of 5 l/min against a differential pressure of 100 mmHg when rotated at 1700 rpm, as shown in Fig. 14a. Under these conditions, the total power consumption, shown in Fig. 14b, was 5.5 W (P_{motor} = 4.0 W and P_{mb} = 1.5 W), and the pump efficiency, as shown in Fig. 14c, was 20%.

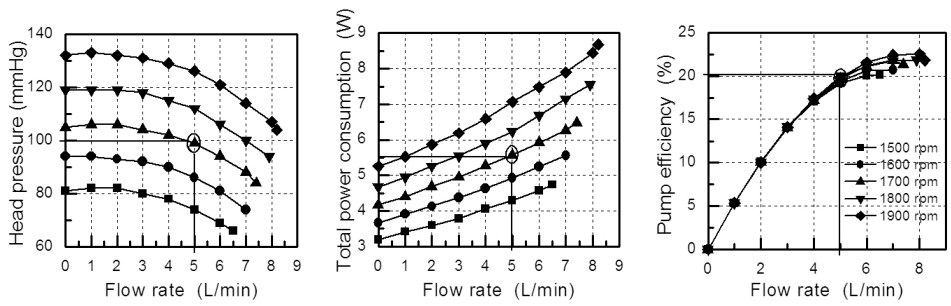

(a) (b) (c)

Fig. 14 Pump performance (a) pressure-flow curve, (b) total power consumption and (c) pump efficiency

The MB of a MedTech Heart with a titanium housing had the same power consumption as one with a plastic housing, 1.5 W, showing that the eddy current loss generated on the surfaces of the stator wall and the impeller cover were low, and had little influence on the power consumption of the MB.

Comparing the total pump efficiency of the MedTech Heart in a titanium housing with one in a plastic housing, there was a decrease in efficiency from 21% to 20%. The loss due to eddy currents in the motor is also small. However, compared with a pump without signal conditioning, an increase in pump efficiency from 6.7% to 20% was observed.

5.2 Hemolytic characteristics of the pump

The hemolytic performance was tested with the centrifugal blood pump connected to a mock circulatory loop. The experiment was performed using fresh porcine blood, anticoagulated with a mixture of citric and dextran solution, collected from a slaughterhouse on the same day of the experiment and refrigerated during transportation. Five identical experiments (n = 5) were performed, each using 500 ml of blood maintained at 37 degrees Celsius by immersing the tubing and reservoir in a water bath. The pump was set to deliver a flow of 5 l/min against a head pressure of 100 mmHg for four hours. The hemolytic levels, represented by the Normalized Index of Hemolysis (NIH), of a MedTech Heart in a titanium housing were compared to those of a Bio-Pump BPX-80, under identical experimental conditions. To calculate NIH, three blood samples were taken at 0 hours (beginning) and at four hours (end of experiment) to evaluate the variation of the free hemoglobin level. The NIH was calculated using the formula (7)

$$\mathrm{NIH} = \Delta freeHb \times V \frac{100 - Ht}{100} \frac{100}{Q\ T} \tag{7}$$

where $\Delta freeHb$, obtained from the mean value of three samples, is the increase in the plasma free hemoglobin concentration (g/l) over the sampling time interval T (min), V is the circuit volume (l), Q is the flow rate (l/min) and Ht is the hematocrit (%).

The measured mean NIH values and standard deviations of the MedTech Heart and the BPX-80 were 0.0022 ± 0.0006 g/100 L and 0.0039 ± 0.0022 g/100 L respectively. After four hours of experiment, no thrombus formation was observed inside the mock circulatory loop or inside the pump.

Nishida et al have reported the effect of friction caused by contact bearings on the hemolytic characteristics of a centrifugal ventricular assist device [3]. The lower hemolysis level of the MedTech Heart compared to that of the Bio-Pump BPX-80 is due to absence of a contact bearing.

6. Conclusion

A compact maglev centrifugal blood pump enclosed in a titanium housing for use as a long term implantable blood pump was developed. In order to use eddy current type displacement sensors to feedback a radial positioning signal to the impeller through a conducting wall, the stator wall needs to be thinner than the skin depth. In this case, the magnetic flux of the displacement sensor can pass through the stator wall and reach its target. In addition, to obtain better sensitivity of the displacement sensor, the target cover should be made of a low resistivity material to increase the eddy currents generated on its surface. The possibility of using eddy current type displacement sensors through an intervening conducting wall is not only effective for the development of blood pumps, but also for canned pumps used in the semiconductor industry.

Hydraulic forces inside the blood pump gave rise to axial shifting of the impeller, leading to variations in the amplitude of the rotational positioning signal and consequent loss of control of the rotational speed by the motor driver and low pump efficiency. This loss of control was solved by conditioning the rotational positioning signal with respect to the speed of rotation.

The final configuration of the MedTech Heart in a titanium housing provided a flow rate of 5 l/min against a head pressure of 100 mmHg with a hemolytic level 43.6% lower

than a Bio-Pump BPX-80. Under these conditions, the power consumption was 5.5 W and the pump efficiency was 20%. In future work, thrombus formation inside the pump will be evaluated by in vivo tests in animals.

Acknowledgement

This study was partly supported by Grants-in-Aid for Scientific Research no. 19360073 from the Japan Society for Promotion of Science and Electro-Mechanics Technology Advancing Foundation.

References

(1) Wheeldon, D.R., Mechanical Circulatory Support: State of the Art and Future Perspectives, *Perfusion*, Vol. 18, (2003) pp. 233-243

(2) Asama, J., Shinshi, T., Hoshi, H., Takatani, S., and Shimokohbe, A., A Compact Highly Efficient and Low Hemolytic Centrifugal Blood Pump With a Magnetically Levitated Impeller, *Artificial Organs*, Vol. 30, No. 3 (2006) pp.160-167

(3) Nishida, M., Yamane, T., Maruyama, O., Sankai, Y., and Tsutsui, T., Computational Fluid Dynamic Analysis of the Flow around the Pivot Bearing of the Centrifugal Ventricular Assist Device (Effects of Design Variations of the Washout Hole, the Pivot and the Back Gap), *JSME International Journal, Series C: Mechanical Systems, Machine Elements and Manufacturing*, Vol. 49, No. 3 (2007) pp.837-851

(4) Lavos-Valereto, I.C., Wolynec, S., Deboni, M.C.Z., and Konig Jr, B., In Vitro and In Vivo Biocompatibility Testing on Ti-6Al-7Nb Alloy With and Without Plasma-Sprayed Hydroxyapatite Coating, *Journal of Biomedical Materials Research*, Vol. 58, No. 6 (2001) pp.727-733

(5) Zhang, F., Huang, N., Yang, P., Zeng, X., Mao, Y., Zheng, Z., Zhou, Z., and Liu, X., Blood Compatibility of Titanium Oxide Prepared by Ion-Beam-Enhanced Deposition, *Surface & Coatings Technology*, Vol. 84, (1996) pp.476-479

(6) Farrar, D.J., Bourque, K., Dague, C.P., Cotter, C.J., and Poirier, V.L., Design Features, Developmental Status, and Experimental Results with the HeartMate III Centrifugal Left Ventricular Assist System with a Magnetically Levitated Rotor, *ASAIO*, Vol. 53, (2007) pp.310-315

(7) Hoshi, H., Shinshi, T., and Takatani, S., Third-generation Blood Pumps with Mechanical Noncontact Magnetic Bearings, *Artificial Organs*, Vol. 30, No. 5 (2006) pp.324-338

(8) Komoda, T., Weng, Y., Nojiri, C., and Hetzer R., Implantation Technique for the DuraHeart Left Ventricular Assist System, *Journal of Artificial Organs*, Vol. 10, No. 2 (2007) pp.124-127

(9) James, N.J., Wilkinson, C.M., Lingard, N.L., van der Meer, A.L., and Woodard, J.C., Evaluation of Hemolysis in the VentrAssist Implantable Rotary Blood Pump, *Artificial Organs*, Vol. 27, No. 1 (2003) pp.108-113

(10) Kobayashi, E., Wang, H.D., Yoneyama, T., and Hamanaka, H., Mechanical Properties and Corrosion Resistance of Ti-6Al-7Nb Alloy Dental Casting. *Journal of Materials Science: Materials in Medicine*, Vol. 9, (1998) pp.567-574

(11) Halbach, K., Design of Permanent Multipole Magnets With Oriented Rare Earth Cobalt Material, *Nuclear Instrument Methods*, Vol. 169, (1980) pp.1-10

(12) Asama, J., Shinshi, T., Hoshi, H., Takatani, S., and Shimokohbe, A., A New Design for a Compact Centrifugal Blood Pump with a Magnetically Levitated Rotor, *ASAIO*, Vol. 50, (2004) pp.550-556

(13) Kuroki, J., Shinshi, T., Li, L., and Shimokohbe, A., A Micro-Magnetic Bearing Using Capacitive Axial Displacement Sensing, *Precision Engineering*, Vol. 30, (2006) pp. 54-62